Tailored laser wakefield acceleration for decaying particles

Chiara Badiali,[1,*] Rafael Almeida,[1] Bernardo Malaca,[1,2] Ricardo Fonseca,[1,3] Thales Silva,[1] and Jorge Vieira[1]
[1]*GoLP/Instituto de Plasmas e Fusão Nuclear, Instituto Superior Técnico, Universidade de Lisboa, 1049-001 Lisboa, Portugal*
[2]*Centro Nacional de Computação Avançada/Deucalion Supercomputer, 1700-066 Lisboa, Portugal*
[3]*DCTI/ISCTE, Instituto Universitário de Lisboa, 1649-026 Lisboa, Portugal*

(Received 27 June 2025; revised 26 November 2025; accepted 11 March 2026; published 27 April 2026)

We introduce a plasma wakefield acceleration scheme capable of boosting initially subrelativistic particles to relativistic velocities within millimeter-scale distances. A subluminal light pulse drives a wake whose velocity is continuously matched to the beam speed through a tailored plasma density, thereby extending the dephasing length. We develop a theoretical model that is generalizable across particle mass, initial velocity, and the particular accelerating bucket being used, and we verify its accuracy with particle-in-cell simulations using laser drivers with energies in the joule range.

DOI: 10.1103/1pp8-qx35

I. INTRODUCTION

The particle physics community is actively considering muon colliders as one possible next step for high-energy physics studies [1]. Muons, like electrons, are fundamental particles, meaning their total energy is available in collisions, unlike hadrons [2–4]. Nonetheless, due to their finite lifetime ($\tau_\mu = 2.2\,\mu$s in the proper frame), muons must be collected, cooled, and rapidly accelerated before a significant number of them decay [5], which is a challenging task for conventional accelerators that use radio-frequency (rf) cavities to accelerate particles. Similarly, pions and kaons, which have even shorter decay times ($\tau_{\pi^\pm} = 26$ ns and $\tau_{k^\pm} = 12$ ns in the proper frame), are nearly impossible to accelerate efficiently with standard rf accelerators [6–8]. Plasma acceleration, with its $\sim$GV/cm gradients [9–12], can boost short-lived beams to relativistic energies before they decay.

The fraction of particles surviving an acceleration process can be estimated as $S \simeq (\gamma_i/\gamma_f)^{\nu_p}$ [7,13], with γ_i and γ_f being the initial and final Lorentz factors, and $\nu_p = (m_p c)/(qE_{\rm acc}\tau_p)$—where m_p is the particle's rest mass, c is the speed of light in vacuum, $E_{\rm acc}$ is the accelerating field, τ_p is the proper lifetime, and q is the particle's charge. For a representative μ^- bunch accelerated from 200 MeV to 1 GeV in a 0.2 GV/cm plasma stage, one expects a loss of $\sim 10^{-6}$ of the initial particles, whereas a 20 MV/m rf linac yields to 1% particles' loss. For π^-, the contrast is stronger: A fraction of $\sim 10^{-3}$ particles decay in a plasma-based accelerator, in contrast to 94% for the rf.

Kaons, pions, and muons are often created with subrelativistic velocities due to their large masses. A possible solution to accelerate these particles is to employ accelerating structures with a subluminal phase velocity [14,15]. One of the first configurations proposed for muon acceleration relied on direct acceleration methods, using two counterpropagating laser beams to control the phase velocity and form a subluminal acceleration structure [14]. Here, we propose a plasma wakefield acceleration method working in a copropagating geometry.

The use of plasma wakefields [16–18] to accelerate subrelativistic particles requires drivers traveling below the speed of light. These drivers are now available due to recent advances in ultrafast optical shaping techniques [19–21]. One example is space-time wave packets [22], which use pre-engineered correlations between wave vectors and frequency to yield shape-invariant electromagnetic wave packets whose intensity peak can propagate with arbitrary velocity. The distance over which these features persist depends on the laser energy [23]. Spatiotemporal laser shaping, particularly flying-focus pulses with programmable focal velocity, enables precise control over the trajectory of the laser intensity peak. These pulses have been employed in theoretical and simulation studies to propose dephasingless laser wakefield acceleration [24], demonstrated experimentally to enable phase-locked injection via ionization-front control [25], and investigated as a strategy to extend acceleration beyond wave breaking through spatiotemporal driver design [26]. More recently, a transverse flying-focus configuration was introduced to mitigate dephasing in ion acceleration by matching the focal spot velocity to the ion velocity [27]. Furthermore, experimental applications of these pulses in plasma are being investigated [28,29]. In this work, we focus on light pulses with fixed subluminal focal velocity ($v_f < c$). Although subluminal drivers can excite wakefields that trap nonrelativistic particles, energy gain is ultimately limited by dephasing as the beam eventually overtakes the slow driver [30,31] before reaching relativistic velocities.

*Contact author: chiara.badiali@tecnico.ulisboa.pt

In this work, we circumvent these limitations by introducing a versatile subluminal-pulse-driven plasma accelerator that, together with a carefully tailored density profile [32–34], efficiently boosts initially subrelativistic particles to relativistic speeds. At that point, traditional wakefield drivers can further boost their energies [35]. The proposed mechanism achieves rapid acceleration across both linear and nonlinear wakefield regimes. We validate our theoretical predictions with particle-in-cell (PIC) simulations with the code OSIRIS [36], demonstrating how muons, pions, and other particles reach relativistic energies within millimeter-scale distances. Our findings suggest that our subluminal-accelerator concept can be used with heavier hadrons, like kaons and protons, and may open possibilities for compact plasma-based accelerators in various high-energy and applied-physics contexts. In the linear regime, the theoretical model extends naturally to positive particles, like antimuons and antipions. We illustrate the concept considering laser energies in the joule range that have already been demonstrated for pulses with spatiotemporal couplings [29].

II. SETUP AND ANALYTICAL MODEL

To investigate the wake excitation driven by a space-time wave packet, we start by showing a simulation of a pulse whose focal velocity is $v_f = 0.96\,c$, central wavelength $\lambda = 0.8\,\mu$m, and normalized vector potential $a_0 \equiv eE_L/m_e c\omega_0 = 3$ as it propagates through a uniform plasma of density $n_0 = 4 \times 10^{18}\,\mathrm{cm}^{-3}$, resulting in $\omega_0/\omega_p = 20$, where ω_0 is the laser frequency, $\omega_p = (n_0 e^2/m_e\epsilon_0)^{1/2}$ is the plasma frequency, e is the elementary charge, m_e is the electron mass, ϵ_0 is the vacuum permittivity, and E_L is the amplitude of oscillation of the laser electric field. All the simulations here were performed using azimuthal-mode-decomposed cylindrical coordinates [37,38]; simulation details are present in Appendix B. Figures 1(a) and 1(b) summarize the key wake features: (1) a longitudinal accelerating field $E_z \simeq 0.2\,\mathrm{GV/cm}$, (2) alternating focusing/defocusing transverse fields $E_x - B_y$, and (3) an accelerating structure that remains stable over the simulated interval.

The structure of the spatiotemporal laser pulse is further detailed in Figs. 1(c) and 1(d). These panels illustrate how the pulse's peak intensity (gray line), having a length on the order of $\sim$20 μm, travels at a subluminal focus velocity $v_f < c$, while the full laser envelope (black line), with a length on the order of $L \sim 500\,\mu$m, propagates at $v_{\mathrm{env}} \sim c$. The full pulse length L and the velocity difference between the full envelope and the focal velocities determine the duration $\Delta t \simeq L/(v_{\mathrm{env}} - v_f)$ over which the structured pulse can sustain effective acceleration.

Although slow beams can be phase-locked within the wakes generated by these subluminal pulses, the effective acceleration length in a uniform plasma is ultimately limited by dephasing [30]. To prolong the dephasing length, we employ a tailored plasma density profile, as plasma density gradients can provide an additional degree of freedom to control the phase velocity [32–34]. It is then possible to obtain phase locking over extended distances by matching this changing wake velocity to the evolving speed of the accelerated beam.

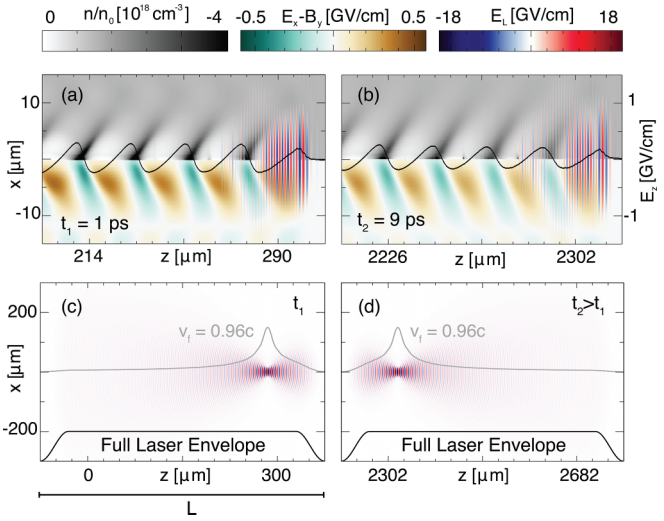

FIG. 1. OSIRIS simulation of a subluminal ($v_f = 0.96c$) spatiotemporal driver pulse in plasma at (a) $t_1 = 1$ ps and (b) $t_2 = 9$ ps. Key features include plasma density (gray), transverse field $E_x - B_y$ (green/orange), on-axis accelerating field E_z (black line), and the laser pulse (blue/red). The wakes are stable, conserving the acceleration structure. In panels (c) and (d), for the same simulation, we show the full laser envelope (black) and the localized intensity peak (gray) that generates the wake (blue-red). Because the envelope travels at c while the focus advances at $v_f < c$, the peak slips backward within the envelope between the two times (c) t_1 and (d) $t_2 > t_1$. Once the peak reaches the envelope tail, the pulse no longer drives efficient wakes.

We can determine the ideal density profile by noting that the accelerating electric field is proportional to the local plasma density $E_z \propto \sqrt{n(z)}$ [39] and imposing that the particle local velocity matches the wake's phase velocity generated by the subluminal driver. We then obtain a system of coupled equations (more details in Appendix A)

$$\frac{d[\gamma(z)v(z)]}{dz} = \alpha_0 \frac{q}{e}\frac{m_e}{m_p}\frac{c}{v_f}\omega_{p0}\sqrt{\frac{n(z)}{n_0}}, \tag{1a}$$

$$v = v_f - \frac{2\pi n_w v_f^2}{\omega_{p0}}\frac{d}{dz}\sqrt{\frac{n_0}{n(z)}}, \tag{1b}$$

where $v(z)$ is the accelerated particle velocity, $\gamma \approx (1 - v(z)^2/c^2)^{-1/2}$ is the Lorentz factor, n_0 is a reference plasma density (here, we use as the initial plasma density of the ideal profile), ω_{p0} is the plasma frequency for the n_0 density, α_0 is the electric field magnitude in units of $m_e c\omega_{p0}/e$, q is the charge of the particle, and n_w is the number of the trailing wake where the particle is accelerated.

Solving Eq. (1) yields the ideal, tailored plasma density profile $n(z)$ that preserves phase locking. In practice, the ideal density taper described by Eq. (1) can be closely approximated using experimentally demonstrated techniques, such as the overlap of two Gaussian gas jets with tunable backing pressures [40–43], or by a sequence of linear up/down ramps generated by shock-front targets [44,45]. Figure 2(a) shows numerical solutions of Eq. (1) considering the first wake of acceleration ($n_w = 1$) for beams of different particle masses, each with an initial velocity of $0.94\,c$ and a driver velocity

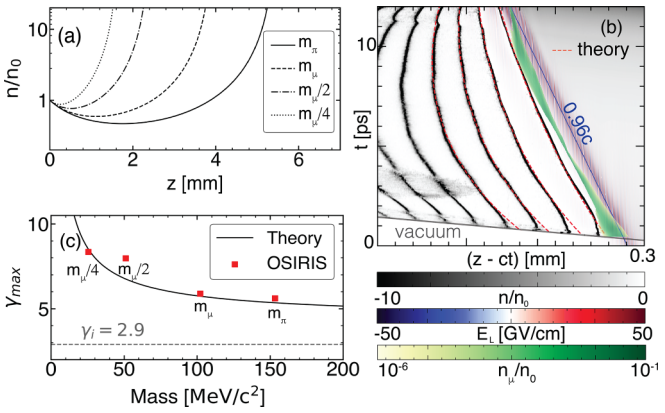

FIG. 2. Overview of our subrelativistic acceleration scheme for muons, pions, and artificially scaled muon masses, all initially at $0.94\,c$ and driven by a driver moving at $0.96\,c$: (a) Tailored plasma density profiles used in simulations for different species, starting with a decreasing density region to capture the subrelativistic beams, followed by an up-ramp that extends phase lock and acceleration. (b) Waterfall plot of the driver and plasma response for muon acceleration, revealing how the density ramps (gray scale) slow down or speed up the wake while the structured pulse (in red/blue) maintains its subluminal velocity at $0.96\,c$. This combination of fixed driver speed and density shaping allows the muon witness beam (in green) to keep phase locking, transitioning smoothly to relativistic velocities within a single acceleration stage. (c) Final maximum γ factor for each particle beam; solid lines are theoretical predictions, and red squares are OSIRIS simulation results.

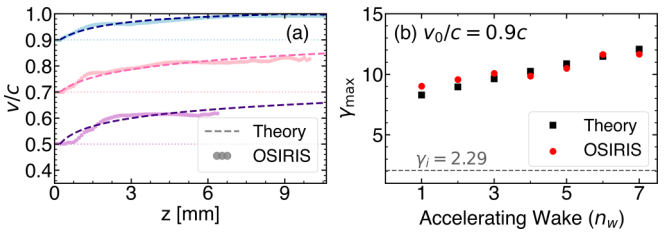

FIG. 3. (a) Maximum velocity evolution v/c of three beams starting at $v_0/c = 0.5$, $v_0/c = 0.7$, and $v_0/c = 0.9$. Each beam is driven with focus velocities of $0.8\,c$, $0.9\,c$, and $0.97c$, respectively. The dashed lines represent the theoretical velocity evolution, and the solid markers are from OSIRIS simulations. (b) Maximum energy γ reached by an $m_\mu/4$ beam initially at $0.9\,c$, accelerated in different wakes by a driver at $0.97\,c$. The black squares are theoretical predictions from our density-tailoring model, and the red circles are OSIRIS simulation results.

of $0.96\,c$. They share a similar structure: An initial downward slope decelerates the back of the accelerating bucket, allowing the beam to be trapped and begin accelerating.

Since the driver's velocity is slightly higher than the beam's, the slope can remain gentle, which mitigates (but does not preclude) electron self-injection, thereby preventing any substantial reduction of the accelerating field. Next, to prevent dephasing as the beam velocity reaches the driver's focal speed, Eq. (1) predicts a region of increasing plasma density that decreases the wakefield wavelength and maintains phase locking. Eventually, the process will be limited by the beam overtaking the driver.

III. PIC VALIDATION AND SCALING

The proposed theory has been tested through self-consistent PIC simulations. Considering the ideal plasma density profile for the muon beam [Fig. 2(a)], Fig. 2(b) shows a waterfall plot of the plasma density and the laser driver electric field as a function of time, along the propagation direction on axis. The sequence of alternating lighter and darker regions behind the driver represents electron density void and accumulation. We notice that the trajectory associated with the regions where electrons accumulate slows down in down-ramp regions and speeds up in up-ramp regions, while the structured light pulse focus propagates at a nearly constant velocity. Figure 2(b) also shows that the phase velocity of the acceleration buckets depends on their distance relative to the driver. These bucket-velocity changes are smaller (higher) for buckets closer to (farther from) the driver. This suggests that buckets farther behind the driver could be beneficial to trap slow particles [15].

Figure 2(c) shows a comparison of the maximum particle energy obtained from simulations and theoretical predictions as a function of the particle mass. The theoretical line is calculated using Eq. (1) by estimating the dephasing time as the time it takes for the beam to reach the laser intensity peak.

We perform simulations for particles of different masses, always injecting the beam particles with the same initial velocity $0.94\,c$, behind a laser driver whose intensity peak travels slightly faster at a focal velocity $v_f = 0.96\,c$. For each particle mass, the plasma is initialized using the optimal density profile calculated from Eq. (1). We observe a good agreement between the theoretical line and the simulation results, demonstrating that our concept is robust for a wide range of particle masses. The simulation parameters used to perform these simulations are summarized in Appendix B.

We also explored the acceleration of beams with different initial velocities. For beam particles with $m_p = m_\mu/4$, we performed simulations with initial beam velocities of $0.5\,c$, $0.7\,c$, and $0.9\,c$, with a corresponding driver velocity of $0.8\,c$, $0.9\,c$, and $0.97\,c$, respectively. The remaining laser parameters in this case are the same as in Fig. 1 but with $a_0 = 0.8$. In Fig. 3(a), the dashed lines show the velocity evolution (v/c) predicted by our model [Eq. (1)], while the solid markers are the maximum particle velocity from the PIC simulations, resulting in a good agreement for all cases.

Equation (1) also predicts the ideal plasma profile as a function of the bucket position n_w. Figure 3(b) shows the final γ factor reached by beams accelerated in the first seven buckets behind the driver, considering $m_p = m_\mu/4$. We use the same configuration as for the blue curve in Fig. 3(a) (beam initially moving at $0.9\,c$ and the driver at $0.97\,c$). Because a later plasma bucket reacts more strongly to a given density variation than the first, its phase velocity also drops faster than that of the first bucket in a region of decreasing plasma density. Thus, we can use a gentle down-ramp to keep the beam in phase with the accelerating bucket, maintaining a high amplitude of the accelerating field. Although the initial field in a secondary bucket is slightly weaker than that of the first, the mild taper is able to maintain the accelerat-

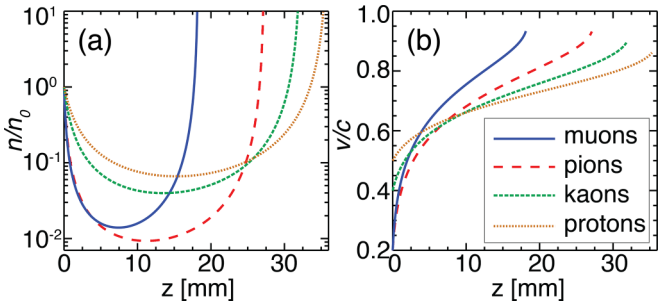

FIG. 4. Density profile [panel (a)] and theoretical velocity gain [panel (b)] for the acceleration of various particles from very low energies (0.2 c for muons and pions, 0.4 c for kaons, and 0.5 c for protons) using a laser driver with $a_0 = 0.8$, $\omega_0/\omega_p = 20$, and $v_f = 0.7\,c$.

ing field. Hence, the beam ultimately gains more energy. In view of potential applications, we also examined the beam loading performance and trapping efficiency of our scheme. We varied the density of the witness beam while maintaining a fixed driver velocity of $0.97\,c$ and a short beam ($\sigma_z \simeq \lambda_p/2$) for the case with initial velocity $v_0 = 0.9\,c$. To characterize the beam loading regime, we introduce the dimensionless parameter $\Lambda = (n_b/n_0)(k_p\sigma_r)^2$ [46]. We investigate three representative cases: $\Lambda = 10^{-5}$ (negligible loading), $\Lambda = 0.13$ (optimal loading), and $\Lambda = 1.3$ (overloading). For $\Lambda = 0.13$, our simulation shows 100% trapping of a 80 pC witness beam. Among the trapped particles, all of them have velocities $v \geqslant 0.97\,c$, 76% reach $v \geqslant 0.98\,c$, and 50% exceed $0.99\,c$. Thus, a large fraction of the accelerated particles have velocities and Lorentz-boosted lifetimes high enough to be suitable for injection into a second-stage accelerator (plasma- or rf-based).

To explore even more demanding scenarios, we extended our theoretical model in Eq. (1) to study the acceleration of heavier particles. Figure 4(a) illustrates the predicted ideal density profile and velocity evolution for these more extreme cases. Figure 4(b) shows that muons, pions, kaons, and protons can be accelerated in tens of millimeters from $v \leqslant 0.5\,c$ to $v \sim 0.9\,c$.

The required laser parameters necessary for the acceleration of these heavier particles are within reach. To show this, we combine an estimate for laser energy with an estimate for the particle energy gain. To determine the laser energy, we first note that the spatiotemporal pulses used here have a transverse Gaussian profile where the full length of the longitudinal envelope is L [see Figs. 1(c) and 1(d)]. Thus, the pulse power P is constant along the pulse, and the pulse energy is $\varepsilon = P\,L/c = \pi\,w_0^2 I_0 L/c$ [47], where $I_0 = c\epsilon_0 E_0^2/2$ is the peak intensity of the laser. One can write an engineering formula for the laser energy as

$$\varepsilon\,[\mathrm{J}] \approx 0.1\,a_0^2\,w_0^2[\mu\mathrm{m}]\,\lambda^{-2}[\mu\mathrm{m}]\,L[\mathrm{mm}]. \tag{2}$$

The total length of the laser envelope L sets the propagation distance over which the localized intensity peak persists within the pulse [see Figs. 1(c) and 1(d)]. The time it takes for the intensity peak to slip backward from the front to the back of the full beam envelope is given by $\Delta t \approx L/(c - v_f)$. Thus, the peak intensity travels a total length $\Delta l \approx \Delta t\,v_f = L\,v_f/(c - v_f)$. These spatiotemporal scales can be seen as analogous to pump depletion for space-time wave packets.

The energy gained by a particle beam in a spatiotemporal pulse acceleration stage can be estimated with $\Delta W = m_p c^2 \Delta\gamma = F\,\Delta l = q\,\langle E_{\mathrm{acc}}\rangle\,L\,v_f/(c - v_f)$, where $\langle E_{\mathrm{acc}}\rangle$ is the average accelerating field. We can rewrite the length L in terms of the energy gain $\Delta\gamma$, focal velocity, particle charge, and $\langle E_{\mathrm{acc}}\rangle$ and replace in Eq. (2), resulting in

$$\varepsilon\,[\mathrm{J}] \approx \frac{a_0^2\Delta\gamma}{20}\frac{e}{q}\frac{m_p}{m_e}\left(\frac{c}{v_f} - 1\right)E_{\mathrm{acc}}^{-1}\left[\frac{\mathrm{GV}}{m}\right]\left(\frac{w_0}{\lambda}\right)^2. \tag{3}$$

With the parameters $a_0 = 0.8$, $w_0 = 3.6\,\mu\mathrm{m}$, $\lambda = 0.8\,\mu\mathrm{m}$, $v_f = 0.97\,c$, and $E_{\mathrm{acc}} = 20\,\mathrm{GV/m}$, the required laser energy to obtain an energy gain of $\Delta\gamma = 5$ is 1, 1.3, 4.9, and 9.2 J for muons, pions, kaons, and protons, respectively. These energy requirements are within the capabilities of state-of-the-art high-intensity laser systems used in advanced laser-plasma experiments [29], supporting the experimental feasibility of this scheme.

IV. CONCLUSIONS

We have shown that subluminal light pulses combined with carefully tailored density profiles can accelerate initially subrelativistic decaying particles (e.g., muons and pions) to relativistic energies over remarkably short distances. We have developed a model to calculate the ideal plasma profile by matching the wake's velocity to the evolving speed of the beam. Our results were validated through numerical simulations, resulting in an excellent agreement in predicting the beam energy gain. Because the scheme operates with few-joule drivers, which have already been demonstrated in spatiotemporal optics experiments [29], exploring plasma-based acceleration of decaying particles is within reach, and it is an application of plasma acceleration that might not have an analog in standard rf accelerators. This approach may serve as a rapid booster stage for decaying particles in muon-collider designs or as a compact source of high-energy pions, kaons, and muons for neutrino physics [48], opening a range of scientific and societal applications. The versatility of the scheme could allow for its application to improve electron acceleration in plasma wakefields and isotope separation.

ACKNOWLEDGMENTS

We acknowledge Luis O. Silva and Pablo Bilbao for fruitful discussions. We gratefully acknowledge EuroHPC for awarding us access to LUMI-C at CSC (Finland). This work was supported by FCT I.P. under Project No. 2024.07895.CPCA.A3 (Grant DOI: 10.54499/2024.06987.CPCA.A3) at MareNostrum 5 supercomputer, jointly funded by EuroHPC JU, Portugal, Turkey, and Spain. This work was supported by the HE EuPRAXIA-PP under Grant Agreement No. 101079773. C.B. acknowledges the support of the Portuguese Science Foundation (FCT) Grant No. PRT/BD/152270/2021 (Grant DOI: 10.54499/PRT/BD/152270/2021), RA FCT Grant No. UI/BD/154677/2022 (Grant DOI: 10.54499/UI/BD/154677/2022), BM FCT Grant No.

PD/BD/150409/2019, and TS FCT IPFN-CEEC-INST-LA3/IST-ID (Grant DOI 10.54499/LA/P/0061/2020).

DATA AVAILABILITY

The data that support the findings of this article are not publicly available upon publication because it is not technically feasible and/or the cost of preparing, depositing, and hosting the data would be prohibitive within the terms of this research project. The data are available from the authors upon reasonable request.

APPENDIX A: TAILORED DENSITY PROFILE

The ideal plasma-density taper that preserves phase synchronism between the accelerated particles and the longitudinal wakefield can be obtained by requiring the instantaneous particle velocity $v(z)$ to coincide with the phase velocity $v_w(z)$ of the n_wth accelerating bucket throughout the interaction length.

The on-axis accelerating field is proportional to the square root of the plasma density and it can be written as

$$E_z(z) = \alpha_0 \frac{m_e \omega_{p0} c}{e} \sqrt{\frac{n(z)}{n_0}}, \tag{A1}$$

where α_0 is the normalized field amplitude. The longitudinal momentum of a test particle of charge q and mass m_p evolves according to

$$\frac{dp_z}{dt} = m_p \frac{d[\gamma(z)v(z)]}{dt} = q E_z(z). \tag{A2}$$

The spatiotemporal driver's peak intensity that is responsible for the wakefield excitation moves at v_f. Thus, we replace the time derivative by the corresponding propagation variable of $z = v_f t$, leading to

$$\frac{d}{dz}[\gamma(z)v(z)] = \alpha_0 \frac{q}{e} \frac{m_e}{m_p} \frac{\omega_{p0} c}{v_f} \sqrt{\frac{n(z)}{n_0}}. \tag{A3}$$

Equation (A3) constitutes the first element of the coupled system that will lead us to our ideal density profile.

The second equation can be derived by noting that each accelerating bucket has an approximate size of $\sim\lambda_p$, the axial position of the center of the n_wth accelerating cavity with respect to the driver peak is

$$\xi_w(t) = v_f t - n_w \lambda_p[z(t)], \quad \lambda_p(z) = \frac{2\pi v_f}{\omega_p(z)}, \tag{A4}$$

with $\omega_p(z) = \sqrt{n(z)e^2/(m_e\varepsilon_0)}$. Differentiation with respect to time gives the phase velocity of the wake

$$\begin{aligned} v_w &= \frac{d\xi_w}{dt} = v_f - n_w v_f \frac{d\lambda_p}{dz} \\ &= v_f - \frac{2\pi n_w v_f^2}{\omega_{p0}} \frac{d}{dz}\sqrt{\frac{n_0}{n(z)}}. \end{aligned} \tag{A5}$$

To obtain the ideal density profile that keeps our particles phase-locked to the ideal acceleration position, we impose that $v_w = v$ when solving Eqs. (A3) and (A5).

APPENDIX B: PIC SIMULATION DETAILS

All simulations were carried out with the fully relativistic PIC code OSIRIS [36] using an azimuthal mode decomposition algorithm with near cylindrically symmetric geometry (r, z–φ), where fields and currents are expanded in azimuthal modes [37,38]. The simulations presented here use the cylindrically symmetric mode ($m = 0$) and $m = 1$, which is enough to capture the laser and wake structure at reduced computational cost. For a nominal plasma density of $n_0 = 4 \times 10^{18}\,\mathrm{cm}^{-3}$, we have $c/\omega_p = 2.55\,\mu\mathrm{m}$. Benchmark simulations were also performed using the azimuthal mode decomposition algorithm with near-cylindrical symmetry, including modes up to $m \leqslant 3$. These tests confirmed that self-injection is already accurately captured with $m \leqslant 1$, with only minimal differences observed when higher modes were included.

The simulation was performed in a window comoving at the speed of light ($\xi = z - ct$) of dimensions $\ell_\xi = 344\,\mu\mathrm{m}$ in the propagation direction and $\ell_r = 51\,\mu\mathrm{m}$ radially, corresponding to $L_\xi = 135\,(c/\omega_p)$ and $L_r = 20\,(c/\omega_p)$. The grid had $27\,000 \times 400$ cells ($\Delta\xi = 0.005\,k_p^{-1}$, $\Delta r = 0.05\,k_p^{-1}$); the time step $\Delta t = 3.5 \times 10^{-3}\,\omega_p^{-1}$ (0.030 fs) satisfied the Courant condition. The simulations had open boundary conditions for outward fields at large r and absorbing conditions for particles. Dynamic load balancing was enabled every 100 iterations.

The driver was a space-time *flying-focus* wave packet centered at $\lambda_0 = 0.8\,\mu\mathrm{m}$ ($\omega_0/\omega_p = 20$), with normalized vector potential $a_0 = 3$ for the cases in Figs. 1 and 2 and $a_0 = 0.8$ in Figs. 3 and 4, spot size $w_0 = 1.4\,k_p^{-1}$ (3.56 μm), and an envelope length $L_{\mathrm{env}} = 108\,k_p^{-1}$ (275 μm). Its intensity peak advanced rigidly at the prescribed focus velocity v_f (Fig. 1), while the envelope propagated at c. In these simulations, the electromagnetic fields of the driver are obtained with a plane wave injection method [49] that satisfies exactly Maxwell's equations, even for strongly nonparaxial wave packets. The fields are continuously injected at the simulation box boundaries throughout the whole simulation. The spatiotemporal spectrum of the wave packet is tuned to result in an intensity focus that moves at the selected subluminal velocity v_f along the propagation axis ("flying focus").

Witness beams were initialized with flat-top shapes with length and radius $\sigma_z = 75\,k_p^{-1}$ (0.2 mm) and $\sigma_r = 0.26\,k_p^{-1}$ (0.5 μm), respectively, peak density $n_b = 10^{-3} n_0$, and particles of mass $m_\pi/m_e = 264$, $m_\mu/m_e = 207$, $m_{\mu/2}/m_e = 100$, and $m_{\mu/4}/m_e = 50$. In these simulations, the witness beam was initialized longer than a single plasma bucket only to avoid fine-tuning its initial position relative to the accelerating phase. In contrast, our theoretical analysis presented in the main text focuses on acceleration in specific buckets to maintain the predicted phase-locking condition and enable efficient acceleration without significant charge loss. The initial velocity of the particle was initialized for different values depending on the case considered. In simulations, the tailored plasma profiles $n(z)$ followed the analytical prescription of Eq. (1) that maintains phase locking while the beam accelerates.

[1] K. R. Long, D. Lucchesi, M. A. Palmer, N. Pastrone, D. Schulte, and V. Shiltsev, Muon colliders to expand frontiers of particle physics, Nat. Phys. **17**, 289 (2021).

[2] A. Costantini, F. De Lillo, F. Maltoni, L. Mantani, O. Mattelaer, R. Ruiz, and X. Zhao, Vector boson fusion at multi-TeV muon colliders, J. High Energy Phys. 09 (2020) 080.

[3] M. Chiesa, F. Maltoni, L. Mantani, B. Mele, F. Piccinini, and X. Zhao, Measuring the quartic Higgs self-coupling at a multi-TeV muon collider, J. High Energy Phys. 09 (2020) 098.

[4] F. Zimmermann, Future colliders for particle physics—"Big and small", Nucl. Instrum. Methods Phys. Res. Sect. A **909**, 33 (2018).

[5] MICE Collaboration, Demonstration of cooling by the muon ionization cooling experiment, Nature (London) **578**, 53 (2020).

[6] G. A. Mourou, T. Tajima, and S. V. Bulanov, Optics in the relativistic regime, Rev. Mod. Phys. **78**, 309 (2006).

[7] T. Goldman and R. R. Silbar, Pion linac as an energy-tagged ν source, Phys. Rev. ST Accel. Beams **11**, 124701 (2008).

[8] H. A. Thiessen, PILAC: A pion linac facility for 1-GeV pion physics at LAMPF, Nucl. Phys. A **547**, 339 (1992).

[9] S. Arjmand, M. Anania, A. Biagioni, M. Ferrario, M. Del Franco, M. Galletti, V. Lollo, D. Pellegrini, R. Pompili, and A. Zigler, Shot-by-shot stability of the discharge produced plasmas in suitably shaped capillaries, J. Instrum. **18**, C04016 (2023).

[10] A. Modena, Z. Najmudin, A. E. Dangor, C. E. Clayton, K. A. Marsh, C. Joshi, V. Malka, C. B. Darrow, C. Danson, D. Neely, and F. N. Walsh, Electron acceleration from the breaking of relativistic plasma waves, Nature (London) **377**, 606 (1995).

[11] M. J. Hogan, C. D. Barnes, C. E. Clayton, F. J. Decker, S. Deng, P. Emma, C. Huang, R. H. Iverson, D. K. Johnson, C. Joshi, T. Katsouleas, P. Krejcik, W. Lu, K. A. Marsh, W. B. Mori, P. Muggli, C. L. O'Connell, E. Oz, R. H. Siemann, and D. Walz, Multi-GeV energy gain in a plasma-wakefield accelerator, Phys. Rev. Lett. **95**, 054802 (2005).

[12] V. Malka, Laser plasma accelerators, Phys. Plasmas **19**, 055501 (2012).

[13] R. J. Noble, Particle production and survival in muon acceleration, AIP Conf. Proc. **279**, 949 (1992).

[14] F. Peano, J. Vieira, R. Mulas, G. Coppa, R. Bingham, and L. Silva, Prospects for all-optical ultrafast muon acceleration, Plasma Phys. Controlled Fusion **51**, 024006 (2009).

[15] A. Pukhov, N. E. Andreev, A. A. Golovanov, I. I. Artemenko, and I. Y. Kostyukov, Controlling wakefield velocity for muon acceleration (beatwave scheme), Plasma **6**, 29 (2023).

[16] T. Tajima and J. M. Dawson, Laser electron accelerator, Phys. Rev. Lett. **43**, 267 (1979).

[17] A. Martinez de la Ossa, J. Grebenyuk, T. Mehrling, L. Schaper, and J. Osterhoff, High-quality electron beams from beam-driven plasma accelerators by wakefield-induced ionization injection, Phys. Rev. Lett. **111**, 245003 (2013).

[18] G. Costa *et al.*, Characterisation and optimisation of targets for plasma wakefield acceleration at SPARC LAB, Plasma Phys. Controlled Fusion **64**, 044012 (2022).

[19] H. E. Kondakci and A. F. Abouraddy, Optical space-time wave packets having arbitrary group velocities in free space, Nat. Commun. **10**, 929 (2019).

[20] D. H. Froula *et al.*, Spatiotemporal control of laser intensity, Nat. Photon. **12**, 262 (2018).

[21] A. Sainte-Marie, O. Gobert, and F. Quéré, Controlling the velocity of ultrashort light pulses in vacuum through spatio-temporal couplings, Optica **4**, 1298 (2017).

[22] M. Yessenov, L. A. Hall, K. L. Schepler, and A. F. Abouraddy, Space-time wave packets, Adv. Opt. Photon. **14**, 455 (2022).

[23] R. Almeida, D. Ramsey, A. F. Abouraddy, J. P. Palastro, and J. Vieira, Universal structure of propagation-invariant optical pulses, Opt. Lett. **50**, 3393 (2025).

[24] J. P. Palastro, J. L. Shaw, P. Franke, D. Ramsey, T. T. Simpson, and D. H. Froula, Dephasingless laser wakefield acceleration, Phys. Rev. Lett. **124**, 134802 (2020).

[25] C. Caizergues, S. Smartsev, V. Malka, and C. Thaury, Phase-locked laser-wakefield electron acceleration, Nat. Photon. **14**, 475 (2020).

[26] J. P. Palastro, B. Malaca, J. Vieira, D. Ramsey, T. T. Simpson, P. Franke, J. L. Shaw, and D. H. Froula, Laser-plasma acceleration beyond wave breaking, Phys. Plasmas **28**, 013109 (2021).

[27] Z. Gong, S. Cao, J. P. Palastro, and M. R. Edwards, Laser wakefield acceleration of ions with a transverse flying focus, Phys. Rev. Lett. **133**, 265002 (2024).

[28] A. Liberman, A. Golovanov, S. Tata, A.-M. Talposi, and V. Malka, Probing flying-focus wakefields, Rep. Prog. Phys. **89**, 038501 (2026).

[29] A. Liberman, R. Lahaye, S. Smartsev, S. Tata, S. Benracassa, A. Golovanov, E. Levine, C. Thaury, and V. Malka, Use of spatiotemporal couplings and an axiparabola to control the velocity of peak intensity, Opt. Lett. **49**, 814 (2024).

[30] J. D. Sadler, C. Arran, H. Li, and K. A. Flippo, Overcoming the dephasing limit in multiple-pulse laser wakefield acceleration, Phys. Rev. Accel. Beams **23**, 021303 (2020).

[31] W. Lu, M. Tzoufras, C. Joshi, F. S. Tsung, W. B. Mori, J. Vieira, R. A. Fonseca, and L. O. Silva, Generating multi-GeV electron bunches using single stage laser wakefield acceleration in a 3D nonlinear regime, Phys. Rev. ST Accel. Beams **10**, 061301 (2007).

[32] A. Pukhov and I. Kostyukov, Control of laser-wakefield acceleration by the plasma-density profile, Phys. Rev. E **77**, 025401(R) (2008).

[33] W. Rittershofer, C. Schroeder, E. Esarey, F. Grüner, and W. Leemans, Tapered plasma channels to phase-lock accelerating and focusing forces in laser-plasma accelerators, Phys. Plasmas **17**, 063104 (2010).

[34] X. L. Xu, F. Li, W. An, T. N. Dalichaouch, P. Yu, W. Lu, C. Joshi, and W. B. Mori, High quality electron bunch generation using a longitudinal density-tailored plasma-based accelerator in the three-dimensional blowout regime, Phys. Rev. Accel. Beams **20**, 111303 (2017).

[35] P.-F. Geng, M. Chen, and Z.-M. Sheng, All-optical muon acceleration with structured laser pulses, Phys. Plasmas **31**, 023109 (2024).

[36] R. A. Fonseca *et al.*, OSIRIS: A three-dimensional, fully relativistic particle in cell code for modeling plasma based accelerators, in *Computational Science—ICCS 2002*, edited by P. M. A. Sloot, A. G. Hoekstra, C. J. K. Tan, and J. J. Dongarra (Springer, Berlin, 2002), p. 342.

[37] A. F. Lifschitz, X. Davoine, E. Lefebvre, J. Faure, C. Rechatin, and V. Malka, Particle-in-cell modelling of laser–plasma interaction using Fourier decomposition, J. Comput. Phys. **228**, 1803 (2009).

[38] A. Davidson, A. Tableman, W. An, F. S. Tsung, W. Lu, J. Vieira, R. A. Fonseca, L. O. Silva, and W. B. Mori, Implementation of a hybrid particle code with a pic description in r–z and a gridless description in ϕ into osiris, J. Comput. Phys. **281**, 1063 (2015).

[39] E. Esarey, P. Sprangle, J. Krall, and A. Ting, Overview of plasma-based accelerator concepts, IEEE Trans. Plasma Sci. **24**, 252 (1996).

[40] G. Golovin, S. Chen, N. Powers, C. Liu, S. Banerjee, J. Zhang, M. Zeng, Z. Sheng, and D. Umstadter, Tunable monoenergetic electron beams from independently controllable laser-wakefield acceleration and injection, Phys. Rev. ST Accel. Beams **18**, 011301 (2015).

[41] G. Golovin, S. Banerjee, S. Chen, N. Powers, C. Liu, W. Yan, J. Zhang, P. Zhang, B. Zhao, and D. Umstadter, Control and optimization of a staged laser-wakefield accelerator, Nucl. Instrum. Methods Phys. Res. Sect. A **830**, 375 (2016).

[42] T. Kurz *et al.*, Demonstration of a compact plasma accelerator powered by laser-accelerated electron beams, Nat. Commun. **12**, 2895 (2021).

[43] Y.-Y. Chang, J. C. Cabadağ, A. Debus, A. Ghaith, M. LaBerge, R. Pausch, S. Schöbel, P. Ufer, U. Schramm, and A. Irman, Reduction of the electron-beam divergence of laser wakefield accelerators by integrated plasma lenses, Phys. Rev. Appl. **20**, L061001 (2023).

[44] K. Schmid *et al.*, Density-transition based electron injector for laser driven wakefield accelerators, Phys. Rev. ST Accel. Beams **13**, 091301 (2010).

[45] A. Buck *et al.*, Shock-front injector for high-quality laser-plasma acceleration, Phys. Rev. Lett. **110**, 185006 (2013).

[46] W. Lu, Nonlinear plasma wakefield theory and optimum scaling for laser wakefield acceleration in the blowout regime, Ph.D. thesis, University of California, Los Angeles (UCLA), 2006.

[47] B. E. A. Saleh and M. C. Teich, Beam optics, in *Fundamentals of Photonics*, edited by B. E. A. Saleh and M. C. Teich (John Wiley & Sons, Ltd, New York, 1991), Chap. 3, pp. 80–107.

[48] A. Apyan, M. W. Krasny, and W. Placzek, Gamma factory high-intensity muon and positron source: Exploratory studies, Phys. Rev. Accel. Beams **26**, 083401 (2023).

[49] R. R. de Almeida, Arbitrarily non-paraxial electromagnetic wave-packets in particle-in-cell codes, Master's thesis, Instituto Superior Técnico, Universidade de Lisboa, Lisbon, Portugal, 2023.